OPERATIONAL MODAL ANALYSIS FOR SIMULATED FLIGHT FLUTTER TEST OF AN UNCONVENTIONAL AIRCRAFT

Özge Süelözgen[1] and Matthias Wüstenhagen[2]

[1]German Aerospace Center (DLR)
Institute of System Dynamics and Control
82234 Wessling, Germany
oezge.sueeloezgen@dlr.de

[2]German Aerospace Center (DLR)
Institute of System Dynamics and Control
82234 Wessling, Germany
matthias.wuestenhagen@dlr.de

Abstract: The framework of this research paper concerns a phenomenon called "flutter" which is a well-known dynamic aeroelastic instability caused by an interaction between structural vibrations and unsteady aerodynamic forces, whereby the level of vibration may trigger large amplitudes, eventually leading to catastrophic failure of the aircraft within a couple of seconds. Flutter prediction and flutter clearance are major issues in the design, development and certification process of an aircraft. Hence, it is mandatory for certification to guarantee that the aircraft is free from flutter throughout the entire flight envelope. Within the framework of the FLEXOP (Flutter Free FLight Envelope eXpansion for ecOnomic Performance improvement) project, an output-only operational modal parameter estimation algorithm in frequency domain has been implemented for monitoring the evolution of the aeroelastic modes for the nearly real-time surveillance of flutter. Therefore an integrated aeroelastic simulation model for the FLEXOP aircraft has been generated.

This paper primarily addresses the application of the frequency-domain output-only Operational Modal Analysis (OMA) method during the simulated flight flutter test of the FLEXOP aircraft. An automatically running modal parameter estimation method called PolyMax will be introduced, which needs the measured responses of the aircraft preprocessed into output spectra. The output-only OMA requires non-deterministic natural and/or operational excitations which are provided by atmospheric turbulence excitation and/or pilot control inputs.

In addition, a straightforward robust flutter analysis method in frequency-domain called μ-V method is presented. Robust flutter analysis deals with aeroelastic (or aeroservoelastic) stability analysis taking structural dynamics, aerodynamics and/or unmodeled system dynamics uncertainties into account [1]. The primary motivation of the robust flutter analysis is that this method allows the computation of the worst-case flutter velocity which can support the flight test program by a valuable robust flutter boundary.

1 INTRODUCTION

Firstly, a brief overview provides an integrated aircraft model for the simulation of the flight flutter test consisting of nonlinear flight mechanical EoMs for the rigid-body motion of the aircraft and linear elastic EoMs describing dynamics due to the flexibility of the aircraft structure. Once the integrated aircraft model and the simulation environment have been introduced, the paper focuses on the frequency-domain output-only modal analysis method PolyMAX. In many cases, only response data are available while the actual loading informations are unknown, but provide the necessary excitation of the structure. In this case where the response data is the only measurement quantity, one speaks of Operational Modal Analysis (OMA). In this paper, PolyMAX operational modal parameter estimator is applied to simulated in-flight data. Furthermore, a robust flutter analysis method in frequency-domain called μ-V method is introduced taking structural dynamics, aerodynamics and/or unmodeled system dynamics uncertainties into account [1]. This approach enables the computation of the worst-case flutter boundary which can support the flight test program by providing an useful robust flutter margin.

Figure 1: Flexop Demonstrator Aircraft [2]

2 INTEGRATED AEROELASTIC MODEL FOR SIMULATION OF THE FLIGHT FLUTTER TEST OF FLEXOP AIRCRAFT

In this section a brief overview of the integrated aircraft model of the FLEXOP aircraft for the simulation of the flight flutter test is given. The inputs for an aero(servo)elastic simulations are generally a (condensed) Finite Element Model (FEM) consisting of the stiffness matrix and the mass matrix (for each mass case), the steady and/or unsteady aerodynamic forces at a specified Mach number, control laws of the Flight Control System (FCS) acting on the control surface deflections and physical properties of the system such as actuator transfer functions [3]. The aerodynamic model is based on the Vortex Lattice Method (VLM) for steady aerodynamics and the Doublet-lattice method (DLM) for unsteady aerodynamics [4]. Further, in-flight disturbances including continuous wind turbulence model with Dryden velocity spectra has been modeled to represent operational conditions during the flight. A detailed description of the integrated aeroelastic model can be taken from [2]. The following figure 2 shows a general organization for simulation of the flight flutter test.
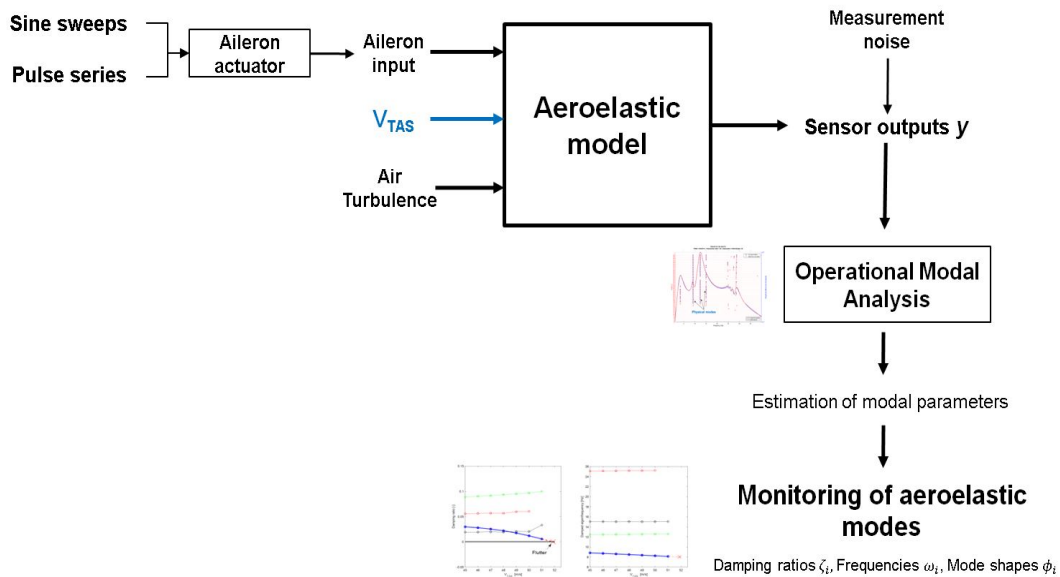
Figure 2: General organization of the aeroelastic system simulation for nearly real-time operational modal analysis

2.1 Structural Dynamics

The interaction of the rigid and elastic-body motion of the aircraft represents the structural dynamics. The rigid-body motion describes the maneuver characteristics of the aircraft, while the elastic-body motion represents the dynamics due to the flexible aircraft structure. A detailed FE model serves as basis for the structural model of the aircraft.

2.2 Finite Element Model

The wing, fuselage and empennage structure is defined by means of a FE model. The FE software used is MSC.NASTRAN. A high-fidelity FE model comprising beam, surface and solid elements represents the wing. Rigid-body interpolation elements, that are added at pre-defined locations along the wing, are used for the Guyan reduction. Beam elements are used to build the fuselage structure. Equivalent beam stiffnesses are obtained at several fuselage cross-sections [5]. Subsequently, the mass is lumped at each beam nodes. The empennage FE model is shell-element based comprising the upper and lower skins, structural rubs, spars and the non-structural masses. A density-based mass representation is used for the empennage as well [2].

By means of a Guyan reduction, also known as static condensation, the aircraft model featuring a very high-fidelity FE model of the wing (more than 600,000 nodes) is reduced to less than 200 nodes. The condensation nodes are distributed along the fuselage beam, the V-tail halves and the left and right wing-box [2].

2.3 Equations of Motion

The rigid body and flexible modes of the condensed model are described by the equations of motion (EOM), which describe the behavior of the aircraft due to external loads, like the aerodynamic and thrust forces. The EOM are based on following assumptions.

1. The earth fixed frame of reference is an interial system, as the earth rotation can be neglected [6].

2. There is no change of gravity throughout the airframe [7].

3. Hooke's law describing linear elastic theory is applicable, due to small deformations of the airframe [6].

4. As a consequence to small deformations of the aircraft structure, the aircraft mass moment of inertia J_b remains unchanged and loads act on the undeformed airframe [6,7].

5. The eigenvectors of the aircraft structure are orthogonal, therefore the total structural deformation can be written as a linear combination of the modal deflections [7].

6. The EOM of the rigid and the flexible body are considered to be decoupled [7].

2.3.1 Rigid Body Motion

The aircraft is considered as a rigid body with a constant mass m_b and constant mass moment of inertia J_b. Based on the specified assumptions the aircraft rigid-body motion is given by the nonlinear Newton-Euler EOM [8]

$$\begin{bmatrix} m_b(\dot{V}_b + \Omega_b \times V_b - T_{be}g_e) \\ J_b\dot{\Omega}_b + \Omega_b \times (J_b\Omega_b) \end{bmatrix} = \Phi_{gb}^T P_g^{\text{ext}}(t). \tag{1}$$

In Equation 1 V_b and Ω_b are the translational and angular velocity of the aircraft with respect to the body frame of reference. The vector g_e represents the gravitational acceleration in an earth fixed frame of reference. By means of T_{be} it is transformed to the body fixed frame of reference. The external loads $P_g^{\text{ext}}(t)$ acting on the entire aircraft structure are summed and transformed into the rigid body frame by the transpose of Φ_{gb}. [6]

2.3.2 Elastic Body Motion

For the elastic motion of the aircraft structure linear elastic theory is used, as the displacement due to the aircraft flexibility is assumed to be small. The effect of the external loads on the structural dynamics is therefore given by the differential equation

$$\mathbf{M}_{ff}\ddot{u}_f + \mathbf{B}_{ff}\dot{u}_f + \mathbf{K}_{ff}u_f = \mathbf{\Phi}_{gf}^T P_g^{\text{ext}}(t), \tag{2}$$

where $\mathbf{M}_{ff}$, $\mathbf{B}_{ff}$ and $\mathbf{K}_{ff}$ are the modal mass, damping and stiffness matrices. The matrix Φ_{gf} contains the eigenvectors of the aircraft structure sorted by frequency [6].

2.4 Aerodynamics

The aerodynamics provide the greatest contribution to the external loads acting on the aircraft structure. The vortex lattice method (VLM) and doublet lattice method (DLM), for which potential theory is applied, are used to model steady and unsteady aerodynamic effects. Both are based on a panel model of the aircraft [6].

2.4.1 Panel Model

The lifting surfaces are discretized by trapezoidal shaped panels, which are also called aerodynamic boxes. The panels of the fuselage are shaped as a T-cruciform. Although this is just a simplification, the fuselage lift distribution matches the solution of a higher-order CFD simulations [2].

2.4.2 Unsteady Aerodynamics via DLM

The unsteady aerodynamics are covered with the DLM. Instead of horseshoe vortices as used for the VLM, doublets are placed at the quarter-chord line of each aerodynamic box. Therefore the pressure coefficients are determined by

$$\Delta c_{pj}(k) = \mathbf{Q}_{jj}(k)w_j(k), \tag{3}$$

where $\mathbf{Q}_{jj}$ is the aerodynamic influence coefficient matrix, w_j is the normalized downwash and k is the dimensionless reduced frequency [6].
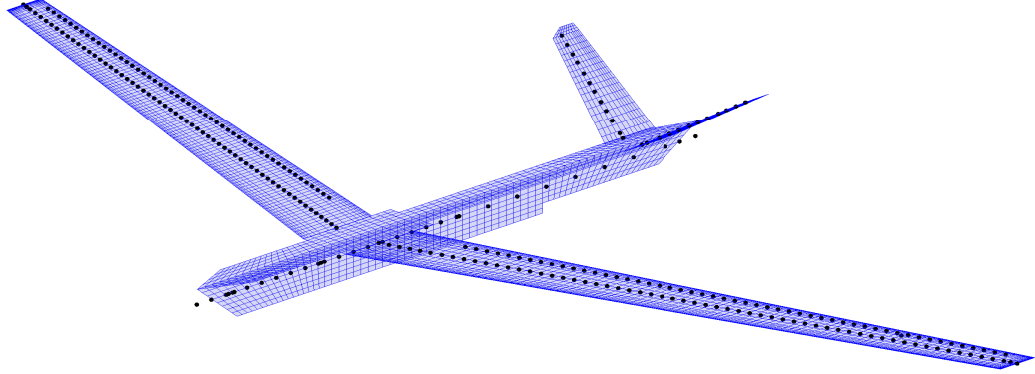

Figure 3: Aerodynamic panel model of the FLEXOP aircraft with structural grids of the condensed FE model

2.5 Wind Turbulence model

For the simulation of the aircraft response to turbulence, Dryden Wind Turbulence Model has been integrated to the aeroelastic simulation model to provide a realistic behaviour of the aircraft in turbulent conditions. The Φ_u, Φ_v and Φ_w components of turbulence are generated according to the Dryden spectra [9], [10], [11] as follows:

$$\Phi_u(\omega) = \frac{2\sigma_u^2 L_u}{\pi V} \frac{1}{1 + \left(L_u \frac{\omega}{V}\right)^2} \tag{4}$$

$$\Phi_v(\omega) = \frac{\sigma_v^2 L_v}{\pi V} \frac{1 + 3\left(L_v \frac{\omega}{V}\right)^2}{\left[1 + \left(L_v \frac{\omega}{V}\right)^2\right]^2} \tag{5}$$

$$\Phi_w(\omega) = \frac{\sigma_w^2 L_w}{\pi V} \frac{1 + 3\left(L_w \frac{\omega}{V}\right)^2}{\left[1 + \left(L_w \frac{\omega}{V}\right)^2\right]^2} \tag{6}$$

where L_u, L_v, L_w are the turbulence scale lengths and σ_u, σ_v, σ_w respresent the turbulence intensities.

5

3 POLYMAX FOR OPERATIONAL MODAL ANALYSIS

In this section theory of the operational modal parameter estimation method PolyMAX will be introduced in short version. It includes preprocessing of the response data into output half spectra, the derivation of the output-only modal model and the deployment of the stabilization diagram.

3.1 Output-only modal model in frequency-domain

Operational Modal Analysis methods in frequency-domain, such as PolyMAX require output spectra as input data. This section will show that under the assumption of white noise input, output spectra can be modelled in a very similar manner as frequency response functions (FRFs). According to the modal theory of mechanical systems the FRF matrix $\mathbf{H}(j\omega) \in \mathbb{C}^{lxm}$ can be modally decomposed as follows [12]:

$$\mathbf{H}(j\omega) = \sum_{i=1}^{n} \frac{v_i l_i^T}{j\omega - \lambda_i} + \frac{v_i^* l_i^H}{j\omega - \lambda_i^*} \tag{7}$$

where n is the number of modes shapes, $[\quad]^*$ is the complex conjugate of a matrix; $[\quad]^H$ is the complex conjugate transpose (Hermitian) of a matrix, $v_i \in \mathbb{C}^l$ are the mode shapes (eigenvectors), $l_i \in \mathbb{C}^m$ are the modal participation factors and λ_i are the poles in complex conjugated form. The modal parameters ω_i (eigenfrequencies) and ζ_i (damping ratios) can now be determined as follows

$$\lambda_i^*, \lambda_i^* = -\zeta_i\omega_i \pm \sqrt{1 - \zeta_i^2} \tag{8}$$

The power spectra of the outputs $\mathbf{S}_{yy}(j\omega) \in \mathbb{C}^{lxl}$ of a dynamic system as a function of the cross power spectra $\mathbf{S}_{uu} \in \mathbb{C}^{mxm}$ of the unknown input forces and the FRF matrix $\mathbf{H}(\mathbf{j}\omega)$ can be defined in a matrix form as follows:

$$\mathbf{S}_{yy}(j\omega) = \mathbf{H}(j\omega)\mathbf{S}_{uu}\mathbf{H}^H(j\omega) \tag{9}$$

In case of operational modal analysis the output spectra are the only available data. The unknown input data are replaced by white noise which has a constant power spectrum and thus the input spectra $\mathbf{S}_{uu}$ are frequency-independent. After the combination of the equations (7) and (9) the modal decomposition of the output spectrum matrix can be expressed in partial fraction form [13]:

$$\mathbf{S}_{yy}(j\omega) = \sum_{i=1}^{n} \frac{v_i g_i^T}{j\omega - \lambda_i} + \frac{v_i^* g_i^H}{j\omega - \lambda_i^*} + \frac{g_i v_i^T}{-j\omega - \lambda_i} + \frac{g_i^* v_i^H}{-j\omega - \lambda_i^*} \tag{10}$$

where $g_i \in \mathbb{C}^m$ are the operational reference factors instead of the modal participation factors. This applies if only output data are available. It should be pointed out that the order of the power spectrum model is twice the order of the FRF model. Note that the right hand side of the equation (10) has to be solved based on measured output (response) data pre-processed into output spectra that depicts the left hand side of the equation (10).

3.2 Pre-processing of the output data

In this subsection, the estimation of the power spectra between the outputs and the reference outputs is discussed. As already mentioned, the auto and cross power spectra $\mathbf{S}_{yy}$ are the primary data for model parameter identification based on (10). The various methods of spectrum estimation are categorized in nonparametric, parametric and subspace methods. Basically, there are two classical nonparametric approaches exist for the estimation of auto and cross power spectra. The periodogram estimator acts directly on the spectra of different time blocks resulting from a division of the time segments. The correlogram method first estimates the correlation functions in the time-domain and next the power spectra are obtained by the DFT of the weighted correlation functions [14].

Within the context of modal analysis the correlogram approach will be preferred. It will be demonstrated that this method has some particular advantages. The correlogram approach starts by estimating the correlation functions:

$$\mathbf{R}_i = \frac{1}{N} \sum_{k=1}^{N-1} y_{k+i} y_k^T \tag{11}$$

The output power spectra $\mathbf{S}_{yy}(j\omega)$ are given by Fourier transforming of the weighted estimated correlation functions:

$$\mathbf{S}_{yy}(j\omega) = \sum_{k=-N_{Lag}}^{N_{Lag}} w_k \mathbf{R}_k e^{-j\omega k \Delta t} \tag{12}$$

where N_{Lag} is the maximum number of time lags at which the correlations are estimated. The number of time lags N_{Lag} is significantly smaller than the number of output samples N. This avoids the statistical variance associated with the higher lags of the correlation estimates [13].

To reduce the effect of leakage the application of an adequate $(2N_{Lag} + 1)$-point time window w_k (e.g. Hamming, Hanning...) symmetric around the origin is recommended [14]. However, the use of a time window introduces bias errors on the final modal parameters. Therefore, an exponential window can be used and thus the bias on the estimated parameters can be corrected. The addition of the artificial damping by the use of the exponential window given by

$$w_k = e^{\frac{k}{N_{Lag}} ln(\frac{P}{100})} \qquad k = 0, 1, ..., N_{Lag} \tag{13}$$

reduces both the influence of leakage and the influence of the stochastic uncertainties [14]. Note that in the equation (13) only the positive time lags are considered. A further advantage of the weighted correlogram within the modal analysis framework is that computing of the so-called half spectra consisting of only correlations having positive time lags in (12) is completely sufficient:

$$\mathbf{S}_{yy}^+(j\omega) = \frac{w_0 \mathbf{R}_0}{2} + \sum_{k=1}^{N_{Lag}} w_k \mathbf{R}_k e^{-j\omega k \Delta t} \tag{14}$$

The half spectra (14) and the full spectra (12) are related as follows:

$$\mathbf{S}_{yy}(j\omega) = \mathbf{S}_{yy}^+(j\omega) + [\mathbf{S}_{yy}^+(j\omega)]^H \tag{15}$$

Furthermore, it is demonstrated in [14] that the modal decomposition of the half spectra $\mathbf{S}_{yy}^+$ only consists of the first two summands in (10):

$$\mathbf{S}_{yy}^+(j\omega) = \sum_{i=1}^{n} \frac{v_i g_i^T}{j\omega - \lambda_i} + \frac{v_i^* g_i^H}{j\omega - \lambda_i^*} \tag{16}$$

In this research paper the weighted correlogram approach in (14) is used for the the estimation of the output half spectra.

3.3 PolyMAX - A modal parameter estimation method

On the basis of the pre-processed output data into output half spectra in (16), the modal model needs to be derived. When comparing the modal decomposition of the FRF matrix $\mathbf{H}(j\omega)$ in (7) and the half spectra $\mathbf{S}_{yy}^+$ in (16), the parametrization can be performed in a same manner. As a result, the exactly same modal parameter identification methods can be applied in both cases [12].

The the PolyMAX method needs output spectra as primary data in case of output-only data and identifies a right matrix-fraction model:

$$\mathbf{S}_{yy}^+(j\omega) = \sum_{r=0}^{p} z^r [\beta_r] \left(\sum_{r=0}^{p} z^r [\alpha_r] \right)^{-1} \tag{17}$$

where $[\beta_r] \in \mathbb{C}^{lxm}$ are the numerator matrix polynomial coefficients; $[\alpha_r] \in \mathbb{C}^{mxm}$ are the denominator matrix polynomial coefficients and p is the model order. m denotes in this case the number of predefined reference outputs.

Note that in the PolyMAX method, a z-domain model is used. This means that the frequency-domain model is derived from a discrete-time model with polynomial basis functions [12]

$$z_r = e^{j\omega \Delta tr}. \tag{18}$$

where Δ t is the sampling time.

For the modal parameter estimation, only a subspace of the output half spectra $\mathbf{S}_y^+(j\omega)$ is needed, e.g. the cross spectra between all outputs l and a selected limited set of reference outputs m. This corresponds to the selected columns of the half spectra. Accordingly, $\mathbf{S}_y^+(j\omega)$ becomes a $(l\,x\,m)$-matrix instead of a $(l\,x\,l)$-matrix as defined in (9).

The left hand side of the right matrix-fraction model equation given in (17) denotes the measured data (or better: non-parametric estimates). Each row of the right matrix-fraction model can be written as:

$$\forall o = 1, 2, ..., l \quad < S_{y,o}^+(j\omega) >=< B_o(j\omega) > [\mathbf{A}(j\omega)]^{-1} \tag{19}$$

where the numerator row-vector polynomial of output o and the denominator matrix polynomial are defined as:

$$< B_o(j\omega) >= \sum_{r=0}^{p} z_r(j\omega) < \beta_{o,r} > \tag{20}$$

$$[\mathbf{A}(j\omega)] = \sum_{r=0}^{p} z_r(j\omega)[\alpha_r] \tag{21}$$

Assembling of the polynomial coefficients $\beta_{o,r} \in \mathbb{R}^{1xm}$ and $\alpha_r \in \mathbb{R}^{mxm}$ leads to the following expressions:

$$\beta_o = \begin{bmatrix} \beta_{o,0} \\ \beta_{o,1} \\ \vdots \\ \beta_{o,p} \end{bmatrix} \in \mathbb{R}^{(p+1)\,x\,m} \forall o = 1, 2, ..., l \quad , \quad \alpha = \begin{bmatrix} \alpha_0 \\ \alpha_1 \\ \vdots \\ \alpha_p \end{bmatrix} \in \mathbb{R}^{m(p+1)\,x\,m} \tag{22}$$

$$\theta = \begin{bmatrix} \beta_1 \\ \beta_2 \\ \vdots \\ \beta_l \\ \alpha \end{bmatrix} \in \mathbb{R}^{(l+m)(p+1)\,x\,m} \tag{23}$$

The equation (17) is then expanded for each discrete frequency ω_k ($k = 1, 2, ..., N_f$) together with the expressions given in (22) and all unknown model coefficients θ can be calculated as a (weighted) least-squares approximation of these equations. A detailed derivation of this approach can be found in [12].

3.4 Stabilization diagram and pole-residue model

In case of experimental or operational modal analysis, one typically uses a polynomial order which is significantly larger than present in the data to ensure that all dynamics of the structure are captured. This leads to the occurrence of so-called mathematical poles (also called spurious poles). Therefore, an essential part in modal parameter estimation methods comes into effect - a so-called stabilization diagram. Here, the analyzer interaction is required in order to interpret the results from the stabilization diagram to make the distinction between physical and mathematical (spurious) modes by means of using stability criteria for eigenfrequencies, damping ratios and operational reference factors (in case of output-only data).

The evaluation of the results from the stabilization diagram yields a set of (stable) poles and corresponding operational reference factors. The mode shapes can be found by considering the so called pole-residue model:

$$\mathbf{S}_{yy}^+(j\omega) = \sum_{i=1}^n \left(\frac{v_i g_i^T}{j\omega - \lambda_i} + \frac{v_i^* g_i^H}{j\omega - \lambda_i^*} \right) + \frac{1}{j\omega}\mathbf{LR} + j\omega\mathbf{UR} \tag{24}$$

where $\mathbf{LR} \in \mathbb{R}^{lxm}$ is the lower residual and $\mathbf{UR} \in \mathbb{R}^{lxm}$ is the upper residual matrix. These have been included to model the influence of the out-of-band modes within the considered frequency range. The unknown variables $\mathbf{LR}$, $\mathbf{UR}$ and the mode shapes v_i can be obtained by solving (24) in a linear least-squares sense:

$$\underbrace{\left[\mathbf{S}_{yy}^+(\omega_1), \ \ldots \ , \mathbf{S}_{yy}^+(\omega_{N_f}) \right]}_{=\,\mathbf{S}} = \underbrace{\begin{bmatrix} \mathbf{\Phi} & \mathbf{\Phi}^* & \mathbf{LR} & \mathbf{UR} \end{bmatrix}}_{=\,\mathbf{X}} \cdot \underbrace{\begin{bmatrix} \mathbf{\Omega}_1 \mathbf{G}, & \ldots & , \mathbf{\Omega}_{N_f}\mathbf{G} \\ \mathbf{\Omega}_1^* \mathbf{G}^*, & \ldots & , \mathbf{\Omega}_{N_f}^* \mathbf{G}^* \\ \frac{1}{j\omega_1}\mathbf{I}_m & \ldots & \frac{1}{j\omega_{N_f}}\mathbf{I}_m \\ j\omega_1\mathbf{I}_m & \ldots & j\omega_{N_f}\mathbf{I}_m \end{bmatrix}}_{=\,\mathbf{Y}} \tag{25}$$

with

$$\mathbf{\Omega}_k = \begin{bmatrix} \frac{1}{j\omega_k - \lambda_1} & \cdots & 0 \\ \vdots & \ddots & \vdots \\ 0 & \cdots & \frac{1}{j\omega_k - \lambda_n} \end{bmatrix} \in \mathbb{C}^{nxn} \quad \mathbf{\Omega}_k^* = \begin{bmatrix} \frac{1}{j\omega_k - \lambda_1^*} & \cdots & 0 \\ \vdots & \ddots & \vdots \\ 0 & \cdots & \frac{1}{j\omega_k - \lambda_n^*} \end{bmatrix} \in \mathbb{C}^{nxn} \quad (k = 1, 2, ..., N_f) \tag{26}$$

$$\mathbf{G} = \begin{bmatrix} g_1^T \\ g_2^T \\ \vdots \\ g_n^T \end{bmatrix} \in \mathbb{C}^{nxm} \quad \mathbf{G}^* = \begin{bmatrix} g_1^H \\ g_2^H \\ \vdots \\ g_n^H \end{bmatrix} \in \mathbb{C}^{nxm} \tag{27}$$

The equation in (25) can be solved via a psuedo-inverse procedure in a linear least-squares sense:

$$\mathbf{X} = \mathbf{S} \cdot \mathbf{Y}^+ \tag{28}$$

where $\mathbf{Y}^+$ denotes the Moore-Penrose pseudo-inverse matrix of $\mathbf{Y}$. The first n columns of the matrix $\mathbf{X}$ denote the identified complex mode shapes $\mathbf{\Phi}$.

4 ROBUST FLUTTER ANALYSIS

In this research paper a straightforward robust flutter analysis method in frequency-domain is presented, whereby account is taken of account is taken of the uncertainties in the structural dynamics or, more explicitly, the dynamic stiffness matrix (DSM). The uncertainty description for the aerodynamics considered in this paper is realized by assigning uncertainty to the aerodynamic influence coefficients (AICs). Next, structured singular value (or μ) analysis is applied to determine the worst-case flutter boundary based on the flutter equation and modeled parametric uncertainties. Finally, the proposed approach is successfully applied to the FLEXOP aircraft.

4.1 Equations of motion for the aeroelastic system

The equations of motion for the nominal aeroelastic system in Laplace domain is given as

$$\left[s^2\mathbf{M} + s\mathbf{C} + \mathbf{K} - \frac{1}{2}\rho V^2 \mathbf{Q}(\bar{s}, Ma) \right] \eta(s) = 0 \tag{29}$$

where $\eta(s)$ is the vector of Laplace domain generalized coordinates for m flexible modes, $\mathbf{M}$, $\mathbf{K}$ and $\mathbf{C} \in \mathbb{R}^{m \, x \, m}$ are generalized mass, stiffness and viscous damping matrices respectively belonging to the structural dynamics part of the equation; $\mathbf{Q}(\bar{s}, Ma) \in \mathbb{C}^{m \, x \, m}$ is the generalized unsteady aerodynamic influence coefficient (AIC) matrix which is a function of nondimensional Laplace variable $\bar{s}$ and the Mach number Ma. The variable ρ denotes the density of atmosphere and V is the flight speed. The AIC matrix can be computed by several aerodynamic theories, such as doublet lattice method (DLM). In this paper, the subsonic unsteady aerodynamic forces have been modeled by means of DLM. Based on small disturbance hypothesis, DLM solves the linearized potential flow equation and obtains the aerodynamic forces under the assumption that aerodynamic surfaces oscillate harmonically. The nondimensional Laplace variable $\bar{s}$ is denoted $\bar{s} = g + ik$ where g is the damping and k is the reduced frequency. On the assumption of harmonic aerodynamic loads the nondimensional Laplace variable $\bar{s}$ becomes:

$$\bar{s} = s\frac{c_{ref}}{2V} = i\omega\frac{c_{ref}}{2V} = ik \tag{30}$$

On the basis of the assumption of harmonic oscillations, the flutter equation (29) can be transformed into the frequency-domain as follows

$$\left[-\omega^2\mathbf{M} + i\omega\mathbf{C} + \mathbf{K} - \frac{1}{2}\rho V^2 \mathbf{Q}(ik, Ma) \right] \eta(\omega) = 0 \tag{31}$$

or

$$\left[\mathbf{Z}(i\omega) - \frac{1}{2}\rho V^2 \mathbf{Q}(ik, Ma) \right] \eta(\omega) = 0 \tag{32}$$

where $\mathbf{Z}(i\omega)$ is generalized Dynamic Stiffness Matrix (DSM).

4.2 Uncertainty Modeling in Frequency-Domain

For the realization of the variations in the structural dynamics model of the structure, a frequency-dependent parametric uncertainty in the Dynamic Stiffness Matrix $\mathbf{Z}_S(i\omega)$ has been considered:

$$\mathbf{Z}_S(i\omega) = -\omega^2 \mathbf{M}_S + i\omega \mathbf{C}_S + \mathbf{K}_S \tag{33}$$

where $\mathbf{M}_S$, $\mathbf{C}_S$ and $\mathbf{K}_S \in \mathbb{R}^{N \, x \, N}$ are physical mass, stiffness and viscous damping matrices respectively and N denotes the physical degrees of freedom.

Considering a perturbation of physical Dynamic Stiffness Matrix $\mathbf{Z}_S(i\omega)$, the parametric additive uncertainty can be described as follows:

$$\mathbf{Z}(i\omega) = \mathbf{\Phi}^T \left[\mathbf{Z}_S(i\omega) \, + \, \delta_Z \mathbf{Z}_\Delta(i\omega) \right] \mathbf{\Phi} \tag{34}$$

where, $\mathbf{Z}_S(i\omega)$ is the nominal physical dynamic stiffness matrix and $\mathbf{Z}_\Delta(i\omega)$ is frequency-dependent weigthing matrix defining the uncertainty level of the DSM. δ_Z, is norm-bounded uncertainty operator with $\|\delta_Z\|_\infty \leq 1$. It should be noted that $\mathbf{\Phi}$ is the modal (eigenvector) matrix of the nominal system. This assumption is reasonable for small perturbations and can be validated by modal correlation analysis between nominal and perturbated system. Inserting $\mathbf{Z}_S(i\omega)$ defined in the equation (33) into the equation (34) yields:

$$\mathbf{Z}(i\omega) = \mathbf{Z}_0(i\omega) \, + \, \delta_Z \mathbf{\Phi}^T \mathbf{Z}_\Delta(i\omega) \mathbf{\Phi} \tag{35}$$

with

$$\mathbf{Z}_0(i\omega) = -\omega^2 \mathbf{M} + i\omega \mathbf{C} + \mathbf{K} \tag{36}$$

where $\mathbf{Z}_0(i\omega)$ is nominal generalized Dynamic Stiffness Matrix (DSM).

For the uncertainty modeling in aerodynamics a model with an uncertain aerodynamic modal participation is defined which can be directly determined from the generalized AIC matrix $\mathbf{Q}(ik, Ma)$ [15]. The parametric uncertainty model can be put in the more general form:

$$\mathbf{Q}(ik, Ma) = \mathbf{Q}_0(ik, Ma) + \mathbf{V}_Q(ik, Ma)\mathbf{\Delta}_Q \mathbf{W}_Q \tag{37}$$

If $q_{0,j}$ denotes the jth column in $\mathbf{Q}_0(ik, Ma)$ and $\mathbf{I}_{m \, x \, 1}$ a $(m \, x \, 1)$ unit vector, the following definitions applies:

$$\mathbf{V}_Q(ik, Ma) = \begin{bmatrix} diag(q_{0,1}) & diag(q_{0,2}) & \cdots & diag(q_{0,m}) \end{bmatrix} \quad \in \mathbb{C}^{m \, x \, (m \cdot m)} \tag{38}$$

$$\mathbf{\Delta}_Q = diag(\delta_1 \mathbf{I}_{mxm}, \delta_2 \mathbf{I}_{mxm}, \cdots, \delta_m \mathbf{I}_{mxm}) \quad \in \mathbb{R}^{(m \cdot m) \, x \, (m \cdot m)} \tag{39}$$

$$\mathbf{W}_Q = diag(w_1\mathbf{I}_{mx1},\ w_2\mathbf{I}_{mx1},\ \cdots,w_m\mathbf{I}_{mx1}) \quad \in \mathbb{R}^{(m\cdot m)\,x\,m} \tag{40}$$

where m denotes the number of modes and $\mathbf{I}_{mxm}$ is a mxm identity matrix. A weight $w_1 = 0.05$ means that a 5% uncertainty is assigned to the first column of $\mathbf{Q}(ik, Ma)$, in other words, 5% uncertainty in the contribution from the first mode can be obtained.

An important benefit of this uncertainty modeling approach is that the uncertainty can be restricted to specific modes. Next, a frequency-domain method called μ-V Method for robust flutter analysis will be introduced.

4.3 The μ-V Method for Robust Flutter Analysis

To apply the structured singular value analysis for robust flutter analysis, the uncertain flutter equation (41) can be obtained by means of introducing of the equations (35) and (37) in equation (32)

$$\left[\mathbf{Z}_0(i\omega) - \frac{1}{2}\rho V^2\mathbf{Q}_0(i\omega)\right]\eta(\omega) = \begin{bmatrix} -\mathbf{I}_m & \frac{1}{2}\rho V^2\mathbf{V}_Q(i\omega) \end{bmatrix}\mathbf{w} \tag{41}$$

The additional inputs signals $\mathbf{w}$ are now introduced into nominal aeroelastic system given in Equation (32) to include the perturbations in Dynamic Stiffness Matrix and generalized AIC matrix to the nominal dynamics in a feedback loop:

$$\mathbf{w} = \mathbf{\Delta}\mathbf{z} \tag{42}$$

with the corresponding output signals $\mathbf{z}$

$$\mathbf{z} = \begin{bmatrix} \mathbf{z}_Z \\ \mathbf{z}_Q \end{bmatrix} = \begin{bmatrix} \mathbf{\Phi}^T\mathbf{Z}_\Delta(i\omega)\mathbf{\Phi} \\ \mathbf{W}_Q \end{bmatrix}\eta(\omega) \tag{43}$$

and total uncertainty matrix $\mathbf{\Delta}$

$$\mathbf{\Delta} = diag(\mathbf{\Delta}_Z,\ \mathbf{\Delta}_Q). \tag{44}$$

In order to determine the flutter loop transfer function matrix $\mathbf{F}(i\omega, V, Ma)$ which relates the signals $\mathbf{w}$ and $\mathbf{z}$ as illustrated in Figure 4, the Equation (41) is transformed into the following form:

$$\eta(\omega) = \mathbf{F}_0^{-1}(i\omega)\begin{bmatrix} -\mathbf{I}_m & \frac{1}{2}\rho V^2\mathbf{V}_Q(i\omega) \end{bmatrix}\mathbf{w} \tag{45}$$

where $\mathbf{F}_0(i\omega)$ is recognized as the nominal flutter transfer function matrix:

$$\mathbf{F}_0(i\omega) = \left[\mathbf{Z}_0(i\omega) - \frac{1}{2}\rho V^2\mathbf{Q}_0(i\omega)\right] \tag{46}$$

The flutter loop transfer function matrix $\mathbf{F}(i\omega, V, Ma)$ can now be derived by inserting the Equation (45) into the Equation (43):

$$\mathbf{F}(i\omega, V, Ma) = \begin{bmatrix} \boldsymbol{\Phi}^T \mathbf{Z}_\Delta(i\omega) \boldsymbol{\Phi} \\ \mathbf{W}_Q \end{bmatrix} \mathbf{F}_0^{-1}(i\omega) \begin{bmatrix} -\mathbf{I}_m & \frac{1}{2}\rho V^2 \mathbf{V}_Q(i\omega) \end{bmatrix} \qquad (47)$$

Once the tranfer function matrix $\mathbf{F}(i\omega, V, Ma)$ has been determined the robust flutter speed V_{rob} can be determined within the μ-framework.

Flutter stability of the uncertain aeroelastic system is now equivalent to stability of the flutter loop illustrated in 4, where the structured uncertainty set is scaled to unity norm-bound constraint, such that $\|\boldsymbol{\Delta}\|_\infty \leq 1$. In this context the system is robustly stable is robustly stable with respect to $\boldsymbol{\Delta}$ if and only if the structud singular value [16]

$$\mu(\mathbf{F}(i\omega, V, Ma)) < 1, \qquad \forall\, \omega \geq 0 \qquad (48)$$

For $\mu < 1$ there is no perturbation within exists that will destabilize the system. This state depicts that the true system dynamics are stable, assumming the nomimal model dynamics with its set of uncertainty operators (modeling errors) are able to capture the dynamic behaviour of the true system.
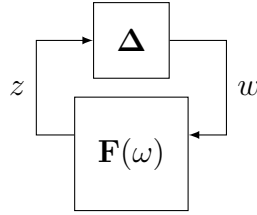

Figure 4: Feedback loop representation of the uncertain flutter transfer function matrix

The robust critical flight speed $V_{flutter}^{rob}$ is reached when any $\mu(\mathbf{F}(i\omega, V, Ma = const.))$ crosses the stability boundary $\mu = 1$. The corresponding algorithm for aeroelastic robust stability analysis is given by the following scheme.

Algorithm 1 Algoritm for robust flutter margin within μ-framework

---

- Compute the flutter speed V_{flut}^{nom} of the nominal system by one of the traditional methods, such as p-k Method

- Initialize a start velocity $V_S < V_{flut}^{nom}$ and calculate $\Delta V = V_{flut}^{nom} - V_S$

- Define a suitable frequency range $\omega = \omega_1, \ldots, \omega_{N_f}$

- Compute $\mu(\mathbf{F}(i\omega, V_S, Ma = const.)) \quad \forall \omega = \omega_1, \ldots, \omega_{N_f}$

- Set tolerance value tol for exit condition

$$\textit{while} \quad \|1 - \max(\mu(\mathbf{F}(i\omega, V_S)))\| > tol$$

$$\Delta V = \frac{\Delta V}{\max(\mu(\mathbf{F}(i\omega, V_S)))}$$

$$V_S = V_S + \Delta V$$

$$\text{Compute } \mu(\mathbf{F}(i\omega, V_S))$$

$$\textit{end}$$

$$V_{flutter}^{rob} = V_S$$

4.4 Numerical Results

For the numerical demonstration, levels and properties of the proposed uncertainty definitions based on the Equations (34) and (37) for the FLEXOP aircraft are listed in the following Table 2.

Table 1: Properties of the uncertainties for the robust flutter analysis

Type	Description	Weighting	Considered modes	Freq. dependency
parametric	physical DSM	$0.025 \cdot \mathbf{Z}_0(i\omega)$	15	yes
parametric	generalized AIC	$0.10 \cdot \mathbf{Q}_0(ik, Ma)$	10	yes

Based on the above defined case, robust aeroelastic analysis results are shown as μ-f-plots at various flight speeds in Figure 5. μ values are taken from the upper bound calculation. The results for the nominal and robust flutter analysis are summarized in Table 2.
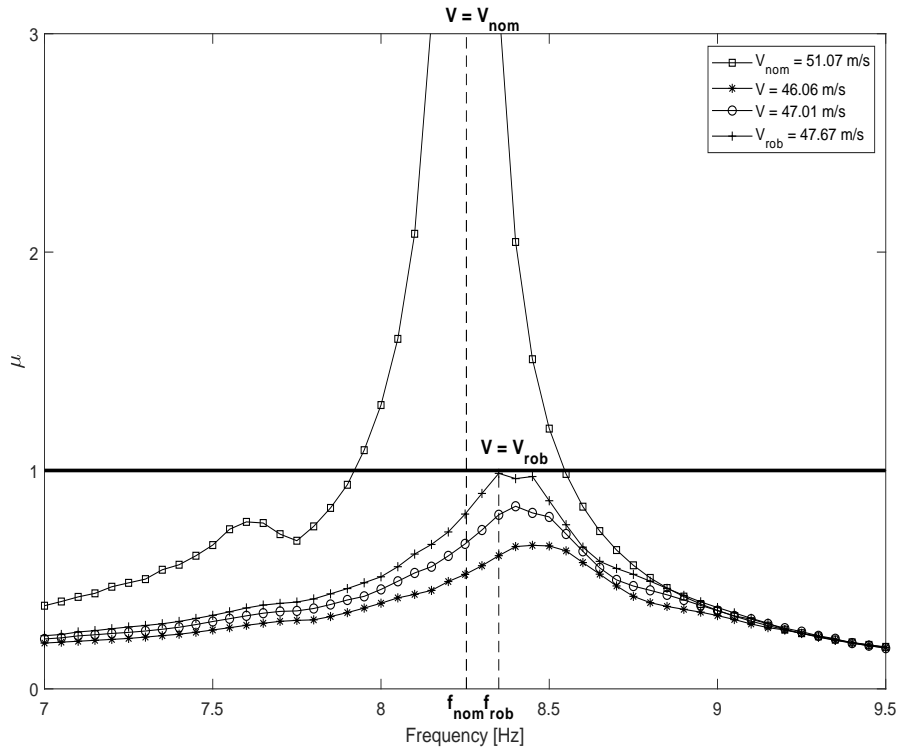
Figure 5: μ-f plots

Table 2: Comparison of nominal and robust flutter analysis results

Method	Type	Aerodynamics	Number of modes	$f_{flutter}$ [Hz]	$V_{flutter}$ [m/s]
p-k	nominal	unsteady (DLM)	15	8.254	51,07
μ-V	robust	unsteady (DLM)	15	8,350	47,67

The numerical example demostrates that even small variation on the Dynamic Stiffness Matrix $\mathbf{Z}(i\omega)$ (only 2,5% of the nominal model) which determines the structural dynamic behaviour of the structure and an uncertain generalized AIC matrix $\mathbf{Q}(ik, Ma)$ with variations on the aerodynamic modal participations of 10% for the first 10 modes, have a major impact on the onset of the flutter. The defined uncertainties reduce the flutter speed by roughly 6.7 % compared to the nominal flutter speed given in Table 2.

5 APPLICATION OF POLYMAX METHOD ON SIMULATED IN-FLIGHT AIRCRAFT DATA

In this section the operational PolyMAX method is applied to simulated in-flight test data of the FLEXOP aircraft. The simulated vibration data have been provided from the integrated aeroelastic model implemented in SIMULINK. The structural deflections of the wings are detected by twelve inertial measurement units (IMUs). At 30%, 60% and 90% span width of each wing an IMU is attached to the front and to the rear spar. In Figure 6 a layout of the IMU positioning is shown.
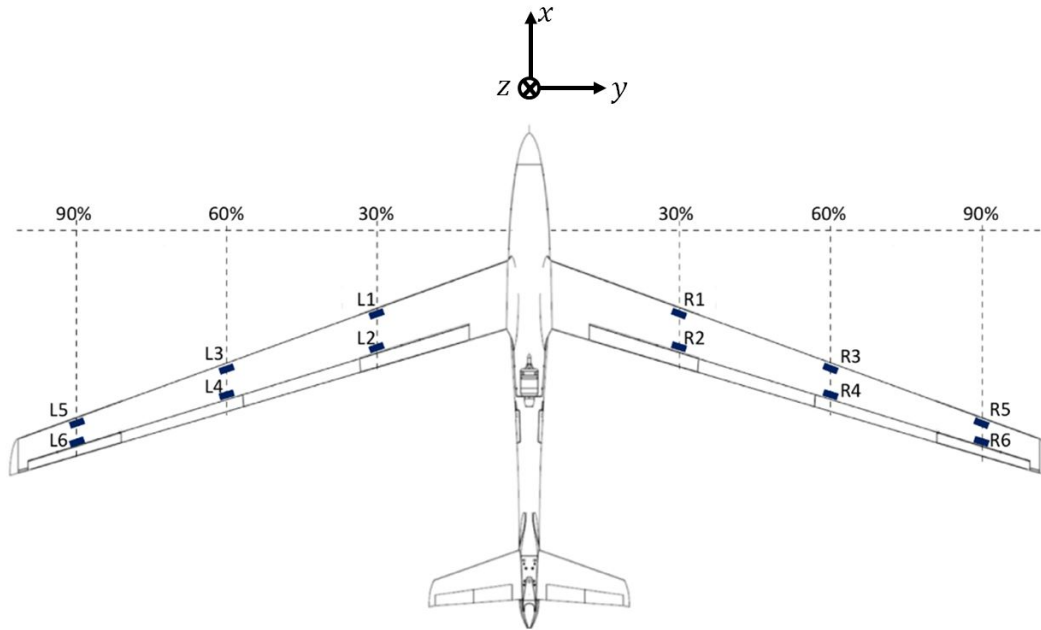
Figure 6: Location of the IMUs

The IMUs measure the translational accelerations in z direction and the angular rates ω_x and ω_y. Therefore, 36 raw time histories (12 x 3 channels) are available for the data analysis.

The simulated vibrations are the structural response to the natural operational excitation modeled via Dryden wind turbulence model. Additionally a pulse excitation by means of doublet input via outer aileron has been applied.

5.1 Analysis and preprocessing of the data set

The simulated raw translational acceleration and angular velocitiy time series are analyzed in time windows of 10 seconds. The original simulation data were sampled at 1000 Hz and are then downsampled to 250 Hz. Two channels are selected as reference outputs and the 36 raw time histories are reduced to a (36 x 2) cross correlation and cross spectrum matrix. An exponential window of 5% has been applied to the cross-correlations before computing the half spectra by means of a Discrete Fourier Transform as shown in the Figures 7 and 8. The number of time lags N_{Lag} at which the correlations have been estimated was 516. The whole preprocess required only 0,96 seconds of computation time.
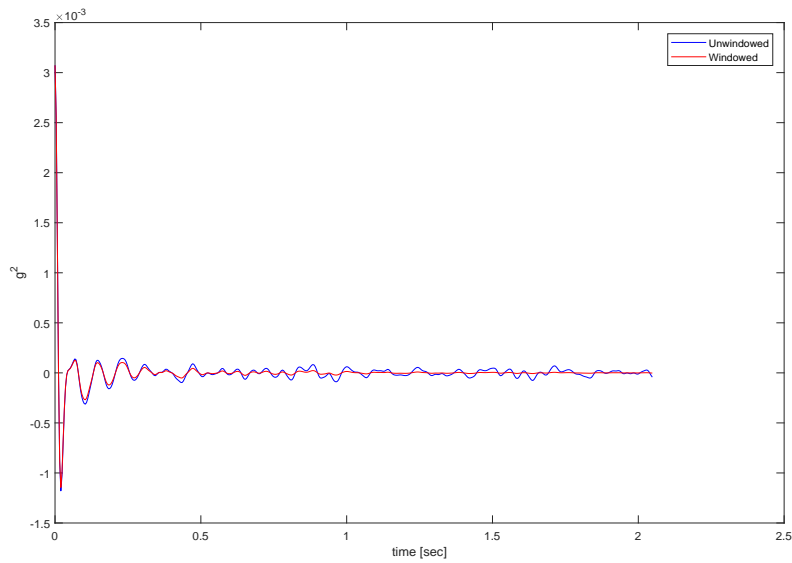
Figure 7: Output correlation before and after applying of exponential window - Sensor R5 in z-direction ($V_{TAS} = 45m/s$)
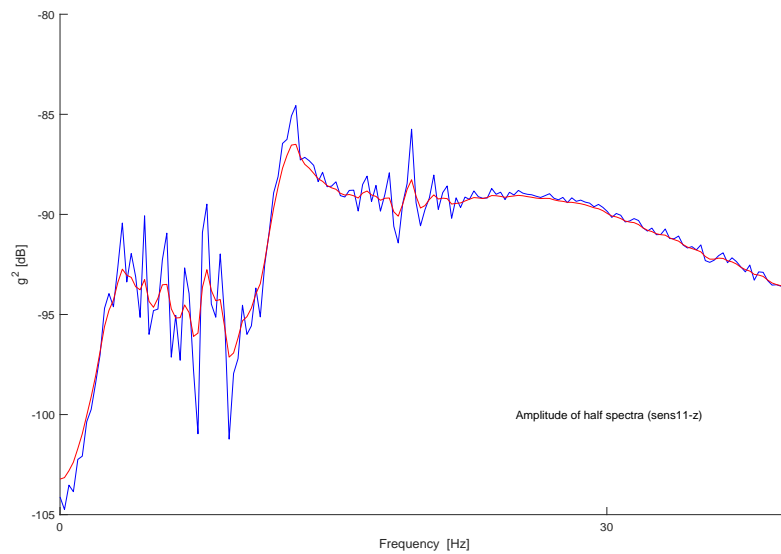

Figure 8: Half spectra before and after applying of exponential window Sensor R5 in z-direction ($V_{TAS} = 45m/s$)

5.2 Applying PolyMAX method to the preprocessed in-flight aircraft data

In this section, the operational PolyMAX method is applied to simulated in-flight aircraft data after preproccesing of the measured (simulated) response data in time domain into the output spectra in order to extract the eigenfrequencies, damping ratios and mode shapes, and tracking the frequency and damping evolution with increasing airspeed (Figure 11). An airspeed range from 45 m/s to 52 m/s has been defined for the monitoring of the onset of the flutter. For each airspeed modal parameters have been extracted. For cleaning of the stabilization diagram followiing criteria have been chosen (Figures 9 and 10):

18

- max. frequency deviation: $1,25\%$
- max. damping ratio deviation: $6,00\%$
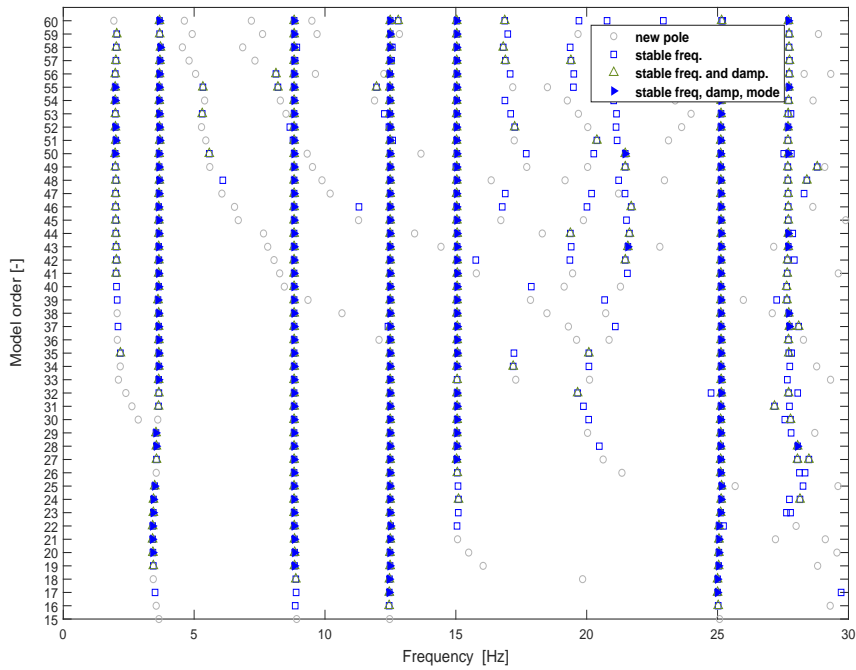- min. MAC (Modal Assurance Criterion): 95%

Figure 9: Uncleaned stabilization diagram (PolyMax)
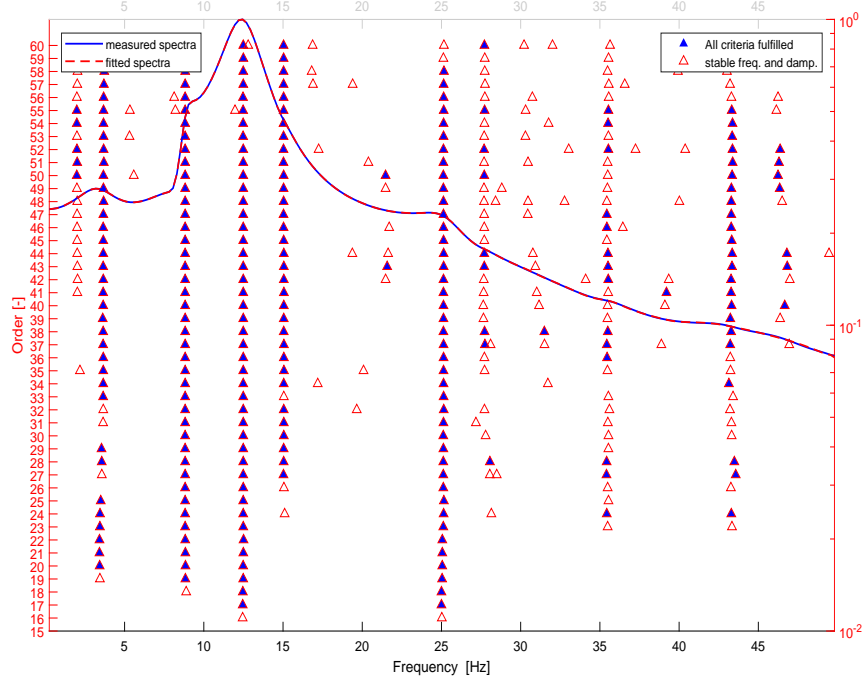

Figure 10: Cleaned stabilization diagram with measured and fitted output spectra (PolyMax)

Figure 11 show the evolution of damped eigenfrequencies and damping values as a function of airspeed, which is the main objective of flight tests.
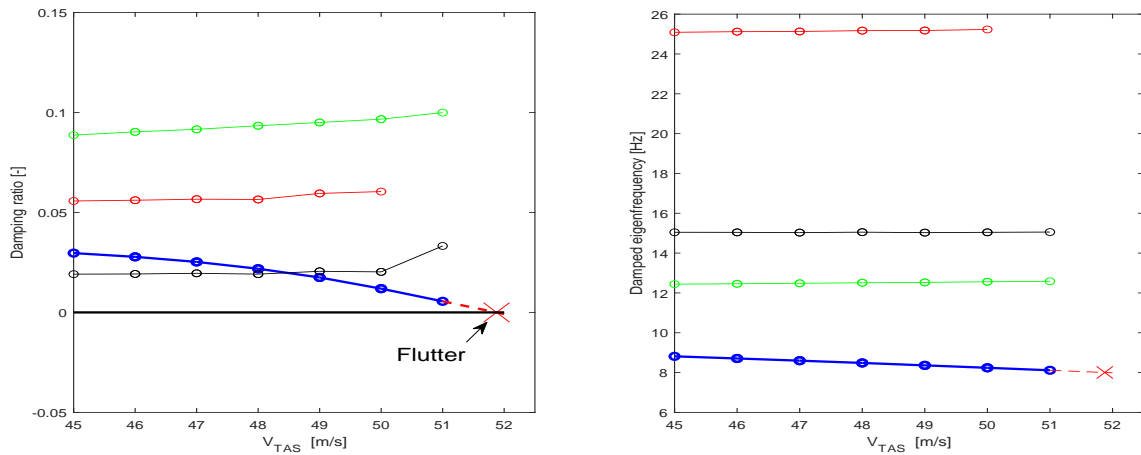

Figure 11: PolyMAX-identified damping ratios (left) and damped natural frequencies (right) with increase of flight speed ($H = 800m$)

The shape of the flutter mode identified with PolyMAX at $V = 51,87 m/s$ is illustrated in Figure 12. Finally, a comparison of the flutter results obtained from online and offline methods is summarized in Table 3.
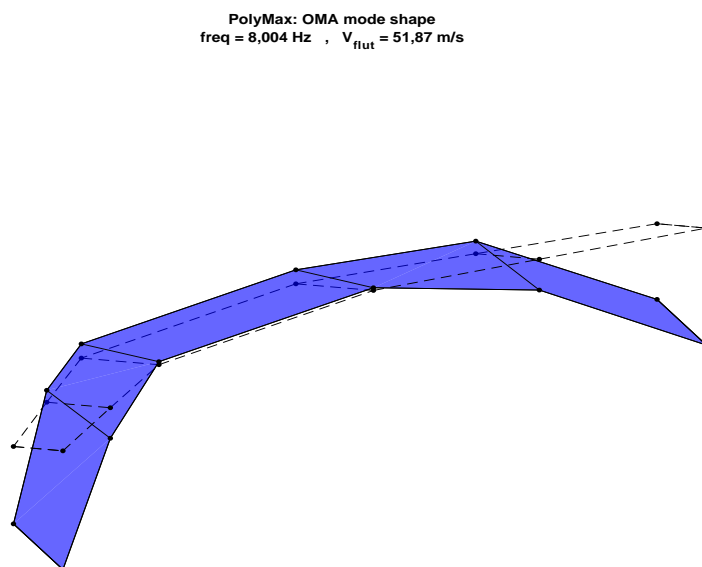

Figure 12: Plot of the flutter mode identified with PolyMax

Table 3: Comparison of flutter results obtained from online and offline methods

Method	Type	$f_{flutter}$ [Hz]	$V_{flutter}$ [m/s]
PolyMAX	online	8,004	51,87
μ-V	offline	8,350	47,67
p-k	offline	8.254	51,07

6 CONCLUSION

Within the framework of the FLEXOP (Flutter Free FLight Envelope eXpansion for ecOnomic Performance improvement) project, an output-only operational modal parameter estimation method, called PolyMAX, for monitoring the evolution of the aeroelastic modes for the nearly real-time surveillance of flutter has been introduced. The application of the PolyMAX method on the simulated flight flutter test data of the FLEXOP aircraft has been succesfully carried out. Furthermore, a robust flutter analysis method in frequency-domain called μ-V method has been presented. It takes structural dynamics, aerodynamics and unmodeled system dynamics uncertainties into account. The primary aim of the robust flutter analysis is that this method allows the computation of the worst-case flutter velocity which can support the flight test program by a valuable robust flutter boundary. The μ-V method is successfully demonstrated on the FLEXOP aircraft.

7 ACKNOWLEDGMENT

8 REFERENCES

[1] Süelözgen, O. (2019). Advanced aeroelastic robust stability analysis with structural uncertainties. *5th CEAS Conference on Guidance, Navigation and Control, April 3-5, 2019, Milano, Italy*.

[2] Wuestenhagen, M., Kier, T., Meddaikar, Y. M., et al. (2018). Aeroservoelastic modeling and analysis of a highly flexible flutter demonstrator. In *2018 Atmospheric Flight Mechanics Conference*. p. 3150.

[3] Kier, T. M. and Looye, G. H. N. (2009). Unifying manoeuvre and gust loads analysis models. *IFASD, The International Forum on Aeroelasticity and Structural Dynamics 2009, Seattle, WA*.

[4] Albano, E. and Rodden, W. (1969). A doublet-lattice method for calculating lift distributions on oscillating surfaces in subsonic flows. *Journal of Aircraft*, 279–285.

[5] Ferede, E. and Abdalla, M. (2014). Cross-sectional modelling of thin-walled composite beams. In *55th AIAA/ASMe/ASCE/AHS/SC Structures, Structural Dynamics, and Materials Conference*. p. 0163.

[6] Kier, T. and Looye, G. (2009). Unifying manoeuvre and gust loads analysis. In *International Forum on Aeroelasticity and Structural Dynamics, No. IFASD-2009-106*.

[7] Reschke, C. (2006). Integrated flight loads modelling and analysis for flexible transport aircraft.

[8] Hofstee, J., Kier, T., Cerulli, C., et al. (2003). A variable, fully flexible dynamic response tool for special investigations (varloads). In *International Forum on Aeroelasticity and Structural Dynamics*.

[9] MIL-HDBK-1797 (1997). Flying qualities of piloted aircraft. *Department of Defense Handbook, Washington, DC: U.S. Department of Defense*.

[10] MIL-F-8785C (2012). Flying qualities of piloted aircraft. *Department of Defense Handbook, Washington, DC: U.S. Department of Defense*.

[11] MIL-HDBK-1797 (1980). Flying qualities of piloted aircraft. *U.S. Military Specification, Washington, DC: U.S. Department of Defense*.

[12] Peeters, B. and der Auweraer, H. V. (2005). Polymax: A revolution in operational modal analysis.

[13] Peeters, B., Vanhollebeke, F., and Van der Auweraer, H. (2007). Operational modal analysis for estimating the dynamic properties of a stadium structure during a football game. *Shock and Vibration*, Volume 14.

[14] Cauberghe, B. (2004). Applied frequency-domain system identification in the field of experimental and operational modal analysis. *Praca doktorska, VUB, Brussel*.

[15] Borglund, D. (2004). The mu-k method for robust flutter solutions. *Journal of Aircraft*.

[16] Lind, R. (1998). *Robust Flutter Margin Analysis that Incorporates Flight Data*. NASA technical paper. National Aeronautics and Space Administration, Dryden Flight Research Center.

COPYRIGHT STATEMENT

The authors confirm that they, and/or their company or organization, hold copyright on all of the original material included in this paper. The authors also confirm that they have obtained permission, from the copyright holder of any third party material included in this paper, to publish it as part of their paper. The authors confirm that they give permission, or have obtained permission from the copyright holder of this paper, for the publication and distribution of this paper as part of the IFASD-2019 proceedings or as individual off-prints from the proceedings.